cancers

MDPI

Article

The Differential Metabolic Signature of Breast Cancer Cellular Response to Olaparib Treatment

Domenica Berardi, Yasmin Hunter †, Lisa van den Driest, Gillian Farrell, Nicholas J. W. Rattray * and Zahra Rattray *

Strathclyde Institute of Pharmacy and Biomedical Sciences, University of Strathclyde, Glasgow G4 0RE, UK; domenica.berardi@strath.ac.uk (D.B.); 2299424H@student.gla.ac.uk (Y.H.); lisa.van-den-driest.2019@uni.strath.ac.uk (L.v.d.D.); gillian.farrell@strath.ac.uk (G.F.)

* Correspondence: nicholas.rattray@strath.ac.uk (N.J.W.R.); zahra.rattray@strath.ac.uk (Z.R.)

† Current address: School of Life Sciences, University of Glasgow, Glasgow G12 8QQ, UK.

Simple Summary: Breast cancer remains a leading cause of female cancer related mortality worldwide. Loss of genomic stability and dysregulation of cellular metabolism are well-recognized features of breast cancer, presenting an opportunity to study the drivers of breast cancer progression and resistance to chemotherapy. The overarching goal of this work is to perform combined analysis of DNA damage repair and cellular metabolism in response to olaparib treatment in a panel of breast cancer cell lines. By applying a combined untargeted metabolomics and molecular biology approach, our findings show dysregulation of amino acid metabolism and metabolic reprogramming from glycolysis to amino acid utilization to be a common feature in all breast cancer cell lines examined, some of which are consistent with findings from the analysis of clinical breast cancer tumours. Functional assessment of genetic alterations offers the scope to design new prognostic tools and inform the design of new chemotherapies or drug combinations.

Abstract: Metabolic reprogramming and genomic instability are key hallmarks of cancer, the combined analysis of which has gained recent popularity. Given the emerging evidence indicating the role of oncometabolites in DNA damage repair and its routine use in breast cancer treatment, it is timely to fingerprint the impact of olaparib treatment in cellular metabolism. Here, we report the biomolecular response of breast cancer cell lines with DNA damage repair defects to olaparib exposure. Following evaluation of olaparib sensitivity in breast cancer cell lines, we immunoprobed DNA double strand break foci and evaluated changes in cellular metabolism at various olaparib treatment doses using untargeted mass spectrometry-based metabolomics analysis. Following identification of altered features, we performed pathway enrichment analysis to measure key metabolic changes occurring in response to olaparib treatment. We show a cell-line-dependent response to olaparib exposure, and an increased susceptibility to DNA damage foci accumulation in triple-negative breast cancer cell lines. Metabolic changes in response to olaparib treatment were cell-line and dose-dependent, where we predominantly observed metabolic reprogramming of glutamine-derived amino acids and lipids metabolism. Our work demonstrates the effectiveness of combining molecular biology and metabolomics studies for the comprehensive characterisation of cell lines with different genetic profiles. Follow-on studies are needed to map the baseline metabolism of breast cancer cells and their unique response to drug treatment. Fused with genomic and transcriptomics data, such readout can be used to identify key oncometabolites and inform the rationale for the design of novel drugs or chemotherapy combinations.

Keywords: breast cancer; triple-negative; oncometabolites; DNA damage; precision medicine; metabolic reprogramming

Citation: Berardi, D.; Hunter, Y.; van den Driest, L.; Farrell, G.; Rattray, N.J.W.; Rattray, Z. The Differential Metabolic Signature of Breast Cancer Cellular Response to Olaparib Treatment. *Cancers* **2022**, *14*, 3661. https://doi.org/10.3390/cancers14153661

Academic Editor: Luisa Alejandra Helguero

Received: 4 July 2022
Accepted: 26 July 2022
Published: 27 July 2022

1. Introduction

In a bid to develop new therapies against various cancer types, and genomic instability, its underpinning mechanisms and contribution to tumorigenesis have been extensively investigated over the past few decades. Genomic instability, a well-known contributor to cancer, presents a therapeutic vulnerability that can be targeted in the development of novel chemotherapy agents [1].

To maintain their genomic integrity, cells are equipped with a range of DNA damage repair (DDR) pathways and responses to counteract DNA lesions formed in response to endogenous and exogenous insults [2]. Hereditary mutations in these pathways have been correlated with increased cancer susceptibility, such that defects in homologous recombination contribute to approximately 10% of all breast cancers. These defects in DDR machinery result in the loss of function for genes implicated in DNA repair (i.e., breast cancer susceptibility gene 1/2—BRCA1/BRCA2) or dysregulation of cell cycle phases [3–5]. While these genetic alterations increase the susceptibility to oncogenesis—they serve as therapeutic vulnerabilities—such that in the presence of a defective DNA repair pathway the inhibition of an alternate DDR mechanism will lead to cell death. This concept is referred to as synthetic lethality, which has formed the rationale for existing DDR inhibitors [6,7]. One such class of drugs, poly(ADP-ribose) polymerase (PARP) inhibitors, target vulnerabilities in the homologous recombination DDR pathway [8].

PARP inhibitors, as a class of DDR inhibitors, block the activity of PARP enzymes involved in DNA damage repair, therefore leading to accumulation of DNA double-strand breaks that gives rise to genomic instability and subsequent apoptosis [9]. Several PARP inhibitors are currently approved as monotherapies for the treatment of locally advanced or metastatic breast cancer for patients, with breast cancer harboring germline BRCA1/2 mutations or HER2-negative receptor status [8]. In 2022, olaparib was approved by the FDA as an adjuvant treatment for patients with human epidermal growth factor receptor 2 (HER2)-negative and germline BRCA-mutated breast cancers following readout from the OlympiA trial [10].

While PARP inhibitors present a therapeutic opportunity for targeting DDR defects in breast and ovarian cancers, emerging evidence has shown a role for oncometabolites—small molecule intermediates of cellular metabolism—in determining the response to these chemotherapies. The biology of oncometabolites and their role in modulating DDR has been increasingly studied over the past few years, guiding new combination therapies and novel biological targets for drug discovery [1].

Metabolic reprogramming—a key feature of all cancers [11]—gives rise to chemoresistance in both treatment-naïve and treatment-resistant breast cancers [12]. As with genomic instability, drivers of metabolic reprogramming can be broadly classified as intrinsic and extrinsic in origin [13]. Intrinsic stimuli, such as oncogenes and tumor suppressor genes, modulate cellular metabolism in breast cancer with several regulators, including BRCA1/2, MYC, phosphatidylinositol-4,5-bisphosphate 3-kinase (PI3K), and p53 as examples. The functional interplay between these regulators of cellular metabolism mediates DNA damage repair pathways and subsequent response to DDR chemotherapies. Recent evidence has shown that the upregulation of glucose utilization and glutamine metabolism are required to sustain increased tumor bioenergetic and biosynthetic demand, which vary according to the cellular genetic makeup [14]. Intermediates from glucose and glutamine metabolism have been identified as key oncometabolites regulating the response to chemotherapy drugs, presenting novel biomarkers and potential actionable targets for novel drug discovery [13].

DDR mechanisms induce cellular metabolic changes through interference with purine and pyrimidine biosynthetic pathways, amino acid metabolism, protein biosynthesis, and energy metabolism, impacting several metabolic routes [15]. Mediators of DDR pathways, including PARP, regulate several pathways exemplified by the pentose-phosphatase pathway, the TCA cycle, and glycolysis. In breast cancer, PARP inhibition reduces glucose consumption and alters amino acid and nucleotide metabolism depending on the

different cellular subtypes [16]. Moreover, BRCA-1 deficient breast tumors appear to rely on glucose consumption through enhanced glycolysis [17]. Differences in the metabolic signature between cell lines harboring different DNA repair mutations and measuring their response to PARP inhibitors can inform the rationale for selecting PARP inhibitors in certain breast cancer types and explore potential additional vulnerabilities as druggable targets [18].

DNA repair and regulation of metabolism is critical for maintaining homeostasis in normal human cells. However, the extensive dysregulation and aberrant function of both these pathways promotes tumorigenesis. Until recently, DNA repair and metabolic pathways have routinely been researched as distinct fields within their own right, but emerging research evidence an intrinsic inter-dependency between these pathways. Here, we report the differential cellular response of breast cancer cell line models with different mutational signatures (see Supplementary Table S1) and DDR defects to olaparib exposure through combined analysis of DNA damage and metabolomics profiling. Combined evaluation of the DNA damage response and metabolic reprogramming offers new opportunities in the development of novel chemotherapies against cancer.

2. Materials

Cell Lines and Chemicals

All cell lines used in this study were purchased from the vendor and maintained in accordance with manufacturer instructions. All cell culture reagents were obtained from Gibco (Thermo Fisher Scientific, Loughborough, Leicestershire, UK). MCF7 (RRID: CVCL_0031, Sigma, EACC collection) and MDA-MB-231 cells (RRID:CVCL_0062, ATCC, Teddington, Middlesex, UK) were purchased and maintained in Dulbecco's Modified Eagle Medium (DMEM, high glucose) supplemented with 10% v/v FBS (high glucose, Invitrogen, Inchinnan, Renfrewshire, UK), 1% v/v non-essential amino acids (NEAA) and 1% v/v penicillin-streptomycin (Invitrogen). Corresponding cell line origins, hormone receptor status and mutational profiles are included in Supplementary Table S1. HCC1937 cells obtained from ATCC (RRID:CVCL_0290) were maintained in RPMI supplemented with 10% v/v FBS and 1% v/v penicillin-streptomycin. All cell lines were maintained at 37 °C in a pre-humidified atmosphere containing 5% v/v CO_2 and used within ten passages for the purposes of this work (passage 2–10). Olaparib (SantaCruz Biotechnology Inc., Wembley, Middlesex, UK) was prepared as a 100 mM stock solution in DMSO, aliquoted, and stored at −20 °C until use. γH2AX, p53BP1 primary antibodies (Cell Signaling Technologies, Danvers, MA, USA), were used for foci immunostaining alongside the Alexa Fluor® 488-conjugated secondary antibody (Fisher Scientific, Loughborough, Leicestershire, UK).

3. Methods

3.1. Cell Viability Assays

MCF-7, MDA-MB-231, and HCC1937 cells undergoing exponential growth were seeded at a density of 4,000 cells/well in 96 well plates and incubated overnight to facilitate cell attachment. On the following day, cells were exposed to either blank growth medium (control) or growth medium containing different concentrations of olaparib (treatment medium) ranging from 0.01–500 μM for seven days at 37 °C and 5% v/v CO_2. Treatment media were replaced every three days with treatment medium. Following a seven-day incubation, cell viability was measured using CellTiter 96® Aqueous Non-Radioactive Cell Proliferation Assay (Promega, Chilworth, Southampton, UK) (3-(4,5-dimethylthiazol-2-yl)-5-(3-carboxymethoxyphenyl)-2-(4-sulfophenyl)-2H-tetrazolium (MTS) reagent. The resultant absorbance at 490 nm was measured using a GM3500 Glomax® Explorer Multimode Microplate Reader (Promega).

Growth curves represent percentage cell growth following treatment with different concentrations of olaparib and are plotted as a semi-log dose–response curve. The half maximal inhibitory concentration (IC_{50}) was determined using a linear regression model.

Statistical analysis was performed using GraphPad Prism (RRID: SCR_002798, v.9.0.1). Three independent biological replicates (five wells per treatment concentration) were performed for each cell line.

3.2. Immunostaining for γH2AX and p53BP1

Foci immunodetection for γH2AX and p53BP1 was performed in both control (growth medium) and for cells treated with olaparib (IC_{10}, IC_{25}, and IC_{50} doses) for seven days. Briefly, cell monolayers were fixed in chilled 4% w/v formaldehyde containing 2% w/v sucrose in PBS, followed by fixation in ice-cold methanol (100% v/v). Subsequently, cells were permeabilized in 0.25% v/v Triton X-100 in PBS, blocked with 5% v/v goat serum/5% w/v BSA, immunoprobed with either a primary rabbit anti-γH2AX antibody (RRID:AB_420030) (1:1000) or primary rabbit anti-P53BP1 (1:200) antibody (RRID:AB_11211252, CST #2675 for p53BP1) overnight at 4 °C. Cell monolayers were treated with goat, anti-rabbit Alexa Fluor® 488 conjugated secondary antibody and counterstained with DAPI. Image acquisition was carried out using an Invitrogen EVOS Auto Imaging System (AMAFD1000-Thermo Fisher Scientific) with a minimum of 100 cells imaged per treatment condition. Resultant foci images were analyzed in Cell Profiler (v.4.2.1.) using a modified version of the speckle counting pipeline.

3.3. Sample Preparation and Metabolite Extraction

MCF-7, MDA-MB-231, and HCC1937 cells were seeded at a density of 2×10^6 cells per well in 6-well plates, and exposed to growth medium containing olaparib at IC_{10}, IC_{25} and IC_{50} doses, as determined from the MTS assay (n = 5 per treatment concentration). Following exposure to olaparib, the growth medium was aspirated from each well, centrifuged to remove cell debris, and stored at −80 °C. Next, treated cells were washed with pre-chilled PBS, with the metabolites quenched and extracted in a final volume of 1.5 mL pre-chilled (−80 °C) mixed solvent (Methanol:Acetonitrile:Water = 50:30:20). Resultant cell pellets were collected, and submerged in liquid nitrogen, vortexed, and sonicated for 3 min in an ice-water bath. This procedure was performed in triplicate. Resultant extracts were centrifuged at 13,000× g for 10 min at 4 °C and the pellets were retained for protein quantification using the Bradford assay. The resultant supernatant was collected and dried with a Speed vac centrifuge (Savant-SPD121P). Dried metabolite pellets were reconstituted in Acetonitrile:Water (50:50) at volumes normalized to the relative protein content. Quality control (QC) samples were prepared by pooling samples across all control and treatment groups. Solvent blank and QC samples were inserted in analytical batch after every five samples to assess the stability of detecting system.

3.4. Liquid Chromatography Tandem Mass Spectrometry (LC-MS/MS)

Metabolite separation was performed on a binary Thermo Vanquish ultra-high performance liquid chromatography system, where 5 µL of reconstituted cellular extract was injected on to a Thermo Accucore HILIC column (100 mm × 2.1 mm, particle size 2.6 µm). The temperature of the column oven was maintained at 35 °C, while the autosampler temperature was set at 5 °C. For chromatographic separation, a consistent flow rate of 500 µL/min was used where the mobile phase in positive heated electrospray ionisation mode (HESI+) was composed of buffer A (10 mM ammonium formate in 95% acetonitrile, 5% Water with 0.1% formic acid) and buffer B (10 mM ammonium formate in 50% acetonitrile, 50% Water in 0.1% formic acid) (Table S2). Likewise, in negative ionization mode (HESI-), buffer A (10 mM ammonium acetate in 95% acetonitrile, 5% water with 0.1% acetic acid) and buffer B (10 mM ammonium acetate in 50% acetonitrile, 50% water with 0.1% acetic acid). The elution gradient used for the chromatographic separation of metabolites is included in supplementary information.

A high-resolution Exploris 240-Orbitrap mass spectrometer (Thermo Fisher Scientific) was used to perform full scan and fragmentation analyses. Global operating parameters were set as follows: spray voltages of 3900 V in HESI+ mode, and 2700 V in HESI- mode. The temperature of the transfer tube was set as 320 °C with a vaporizer temperature of 300 °C. Sheath, aux gas, and sheath gas flow rates were set at 40, 10, and 1 Arb, respectively. Data-dependent acquisitions (DDA) were performed using the following parameters: full scan range was 70–1050 m/z with a MS1 resolution of 60,000. Subsequent MS/MS scans were processed with a resolution of 15,000. High-purity nitrogen was used as nebulising and as the collision gas for higher energy collisional dissociation. Further details are included in supplementary information.

3.5. Mass Spectrometry Data Processing

Raw data files obtained from Thermo Scientific Xcalibur™ software 4.2 were imported into Compound Discoverer™ 3.2 software where the "Untargeted Metabolomics with Statistics Detect Unknowns with ID Using Online Databases and mzLogic" feature was selected (supplementary information). The workflow analysis performs retention time alignment, unknown compound detection, predicts elemental compositions for all compounds, and hides chemical background (using Blank samples). For the detection of compounds, mass, and retention time (RT) tolerance were set to 3 ppm and 0.3 min, respectively. The library search was conducted against the mzCloud, Human Metabolome Database (HMDB) and Chemical Entities of Biological Interest (ChEBI) database. A compound table was generated with a list of putative metabolites (known and unknown). Among them, we selected all the known compounds fully matching at least two of the annotation sources. The selected metabolites were then used to perform pathway and statistical analysis.

3.6. Pathway Analysis with MetaboAnalyst

Prior to analysis of the metabolic pathways with MetaboAnalyst 5.0 (RRID: SCR_015539, https://www.metaboanalyst.ca/, accessed May 6th 2022), a HMDB identification code was assigned to each selected metabolite. A joint pathway analysis was performed by integrating the genes relative to each cell line (Table S1) with the list of ID compounds and their associated Log2 Fold change values. The integration method combined both genes and metabolites into a single query, then was used to perform the enrichment analysis. This latter was based on a hypergeometric test. Finally, important nodes (compounds) were scored based on their betweenness centrality, and pathway analysis results were generated.

3.7. Statistical Analysis

All data are presented as mean ± standard deviation ($n \geq 5$). For cell viability and immunofluorescence quantification data, the Shapiro normality test was performed (Supplementary Table S3). For metabolomics analysis, Principal Component Analysis (PCA) was performed to test analytical reproducibility of QC injections, reduce the dimensionality of our data, and determine the metabolic profiles of the different sample groups. Differential analysis was used to compare differences between control and treatment groups and plotted as a Volcano plot (log-fold change vs. −log10 p-value). Peak areas were log10 transformed and p values were calculated for the sample group by analysis of variance (ANOVA) test. A p value < 0.05 and fold-change of 1.5 was deemed to be statistically significant.

4. Results

4.1. Olaparib Sensitivity Analysis

To determine the olaparib dose range for subsequent foci and metabolomics experiments, we measured the sensitivity of MCF7, MDA-MB-231, and HCC1937 cell lines to

olaparib exposure over a seven-day treatment duration. The rationale behind exploring the sensitivity to olaparib in these cell lines was to perform a comparison between two triple-negative (MDA-MB-231 and HCC1937) and a non-triple-negative (MCF-7) cell line.

Our results show that exposure to olaparib caused a reduction in cell viability in all cell lines in a dose-dependent manner (Figure 1). We observed superior efficacy of olaparib in reducing cell viability in both MCF7 and MDA-MB-231 cells, with a calculated half maximal inhibitory concentration (IC_{50}) of 10 μM and 14 μM, respectively. However, in the case of HCC1937 cells, a higher concentration of olaparib was required to achieve the same reduction in cell viability (150 μM), indicating a lower efficacy of response to olaparib in this cell line.

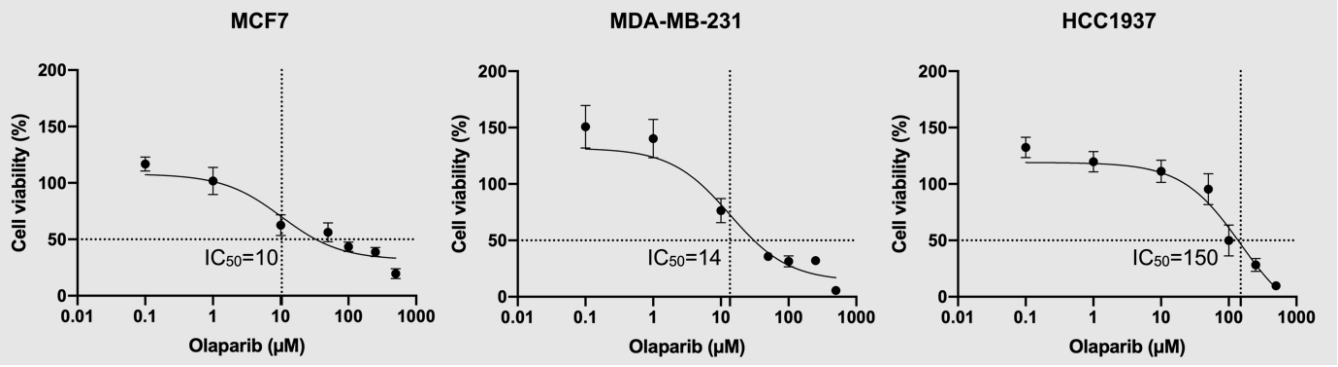

Figure 1. Corresponding MTS dose–response curves for MCF7, HCC1937, and MDA-MB-231 cells treated with ascending doses of olaparib (0.1–500 μM) for seven days. The corresponding R^2 values for fitted dose–response curves in MCF7 (IC_{50} = 10 μM), MDA-MB-231 (IC_{50} = 14 μM), and HCC1937 (IC_{50} = 150 μM) cells were 0.89, 0.91, and 0.85, respectively.

4.2. Exposure to Olaparib Induces Dose-Dependent Formation of γH2AX and 53BP1 Foci in Breast Cancer Cells

PARP inhibition induced by olaparib exposure results in the accumulation of DNA damage in cells by compromising their DDR mechanisms. Therefore, we next investigated the extent to which olaparib exposure at various doses (IC_{10}, IC_{25}, and IC_{50}—determined from MTS assays) promotes the accumulation of DNA double strand breaks (DSBs) in MCF-7, MDA-MB-231, and HCC1937 cell lines. Key markers for DNA DSB formation include phosphorylated histone H2 variant H2AX (γH2AX) [19] and the damage sensor p53-binding protein 1 (p53BP1), which are rapidly recruited to sites of DNA damage and their accumulation is directly proportional to the number of DSB lesions [20]. To measure the extent of DNA DSB formation, we performed immunofluorescence of p53BP1 and γH2AX foci.

Based on our results, p53BP1 and γH2AX foci levels increased in a dose-dependent manner in both MCF7 and MDA-MB-231 cells in response to ascending doses of olaparib (Figures 2a,b,d,e and 3a,b,d,e). However, in HCC1937 cells, a significant increase in foci numbers was not observed in comparison to increased foci numbers with ascending olaparib doses for MCF-7 and MDA-MB-231 cells. the highest olaparib treatment dose (150 μM), in comparison to the 17 and 50 μM exposure doses (Figures S1 c,f and S2 c,f). Generally, a higher number of both p53BP1 (mean > 10 foci per cell) and γH2AX (mean > 20 foci per cell) foci were observed in the HCC1937 cell line, compared to the MCF7 and MDA-MB-231 cells, where a mean of <10 foci per cell were measured for both markers. These results are consistent with the dose-dependent sensitivity of MCF7 and MDA-MB-231 cells in response to olaparib exposure, further confirming cell-line-dependent response to olaparib exposure.

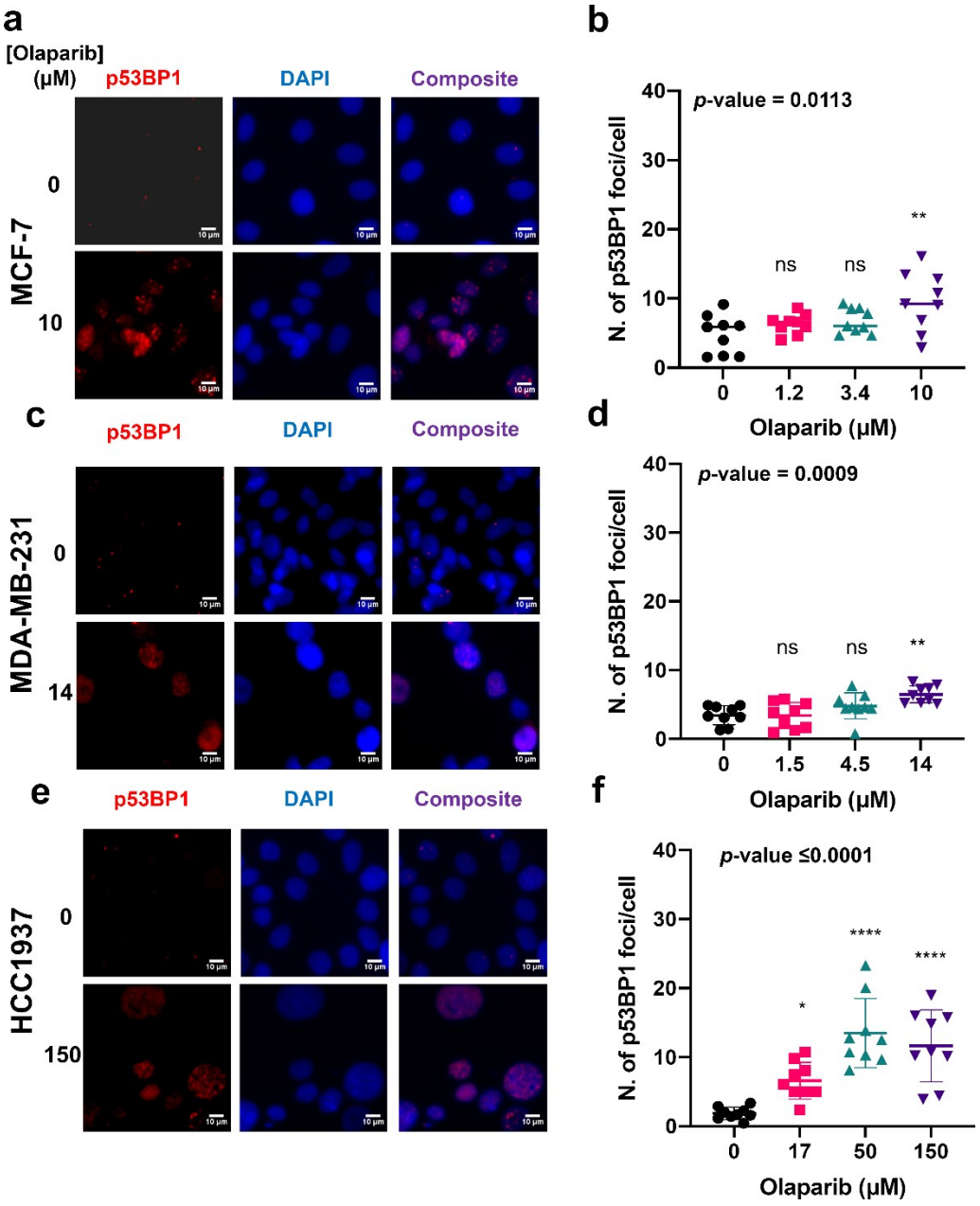

Figure 2. The formation of p53BP1 foci in response to treatment with either growth medium or medium containing olaparib at the IC_{50} dose. Representative images of immunolabelled P53BP1 foci (red), DAPI (blue) nuclear counterstain and composite (p53BP1 (red) and DAPI (blue)) in MCF-7, MDA-MB-231, and HCC1937 cells treated with olaparib for seven days (**a**,**c**,**e**). Corresponding p53BP1 foci counts determined using Cell Profiler (**b**,**d**,**f**). 9 repeats with, on average, > 100 cells per each sample. *p*-values have been determined through ANOVA test. Dunnett's multiple comparison test was used as a follow up to ANOVA test and the *p*-values were represented as: ns, non-significant; *, 0.05; **, 0.005; ****, >0.00005.

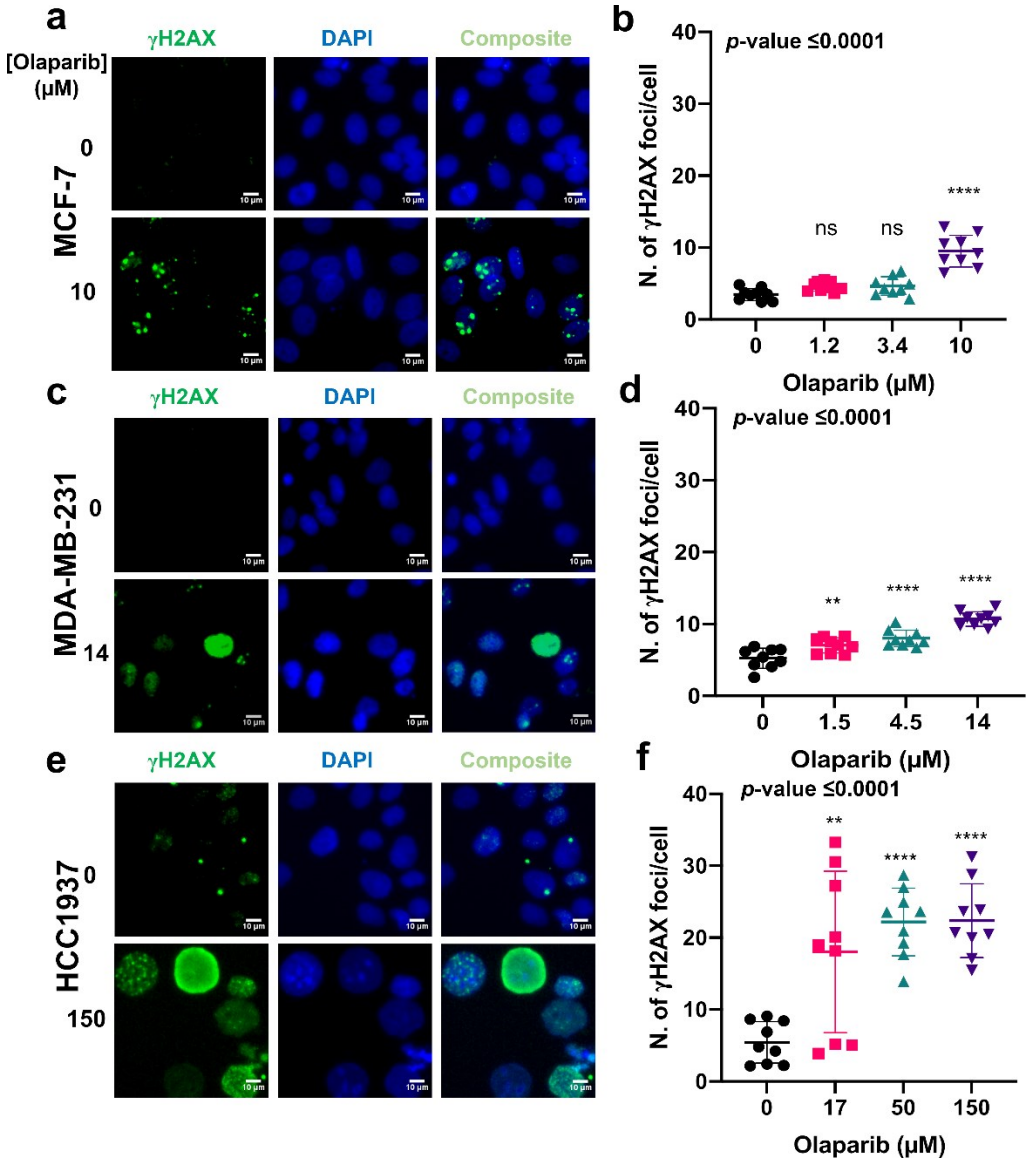

Figure 3. The formation of γH2AX foci formation in response to treatment with either growth medium or medium containing olaparib at the IC_{50} dose. Representative images of immunolabelled γH2AX foci (green), DAPI (blue) nuclear counterstain and composite (γH2AX and DAPI) in MCF-7, MDA-MB-231, and HCC1937 cells treated with for seven days (**a**,**c**,**e**). Corresponding γH2AX foci counts determined using Cell Profiler (**b**,**d**,**f**). (>100 cells per sample). Dunnett's multiple comparison test was used as a follow up to ANOVA and corresponding *p*-values were represented as: ns, non-significant; **, 0.005; ****, >0.00005.

4.3. Biomolecular Pathways Altered in Response to Olaparib Exposure Vary across Different Cell Lines

To comprehensively measure the extent of variation induced by olaparib exposure in MCF-7, MDA-MB-231, and HCC1937 cell lines, we profiled their metabolome using an in-house untargeted liquid chromatography-mass spectrometry-based metabolomics pipeline (Figure S3a). After data acquisition, data processing and analysis were performed in Compound Discoverer 3.2. First, we used principal component analysis (PCA) to visualize and interpret the clustering of quantified metabolite data to examine global differences between treatment groups and cell lines examined, which was followed by pairwise PCA between control and treated groups across positive and negative analysis modes (Figure 4).

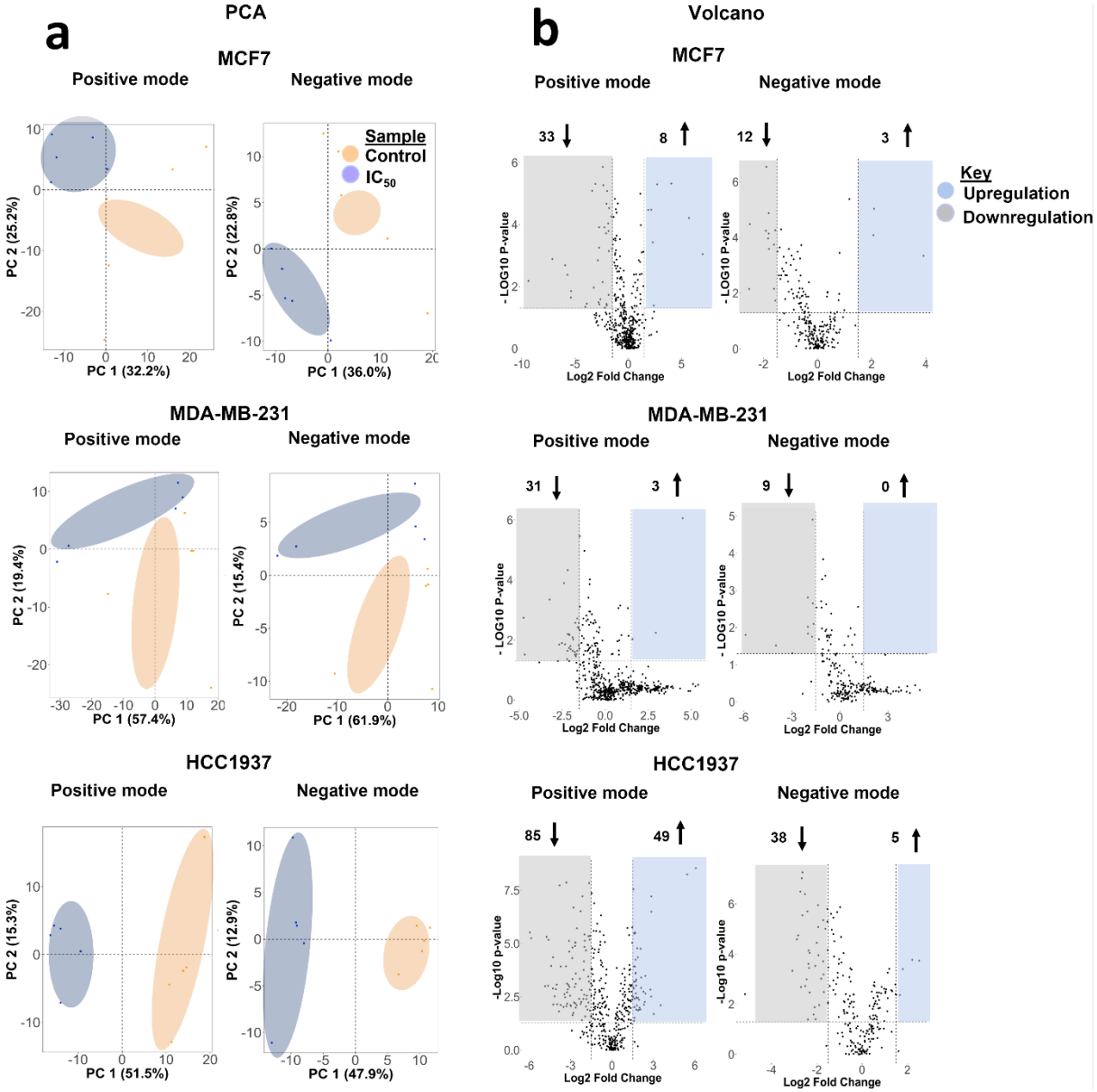

Figure 4. Statistical analyses of global metabolic features identified in MCF7, MDA-MB-231, and HCC1937 upon exposure to the IC_{50} olaparib dose for seven days acquired in positive and negative ionization mode. For each treatment group, five replicates were used. Data points in the two-dimensional PCA score plot were central scaled. (**a**) PCA pairwise analysis and differential analysis of metabolites altered in IC_{50}-treated cells, (**b**) Volcano plots displaying enriched (blue) and depleted (grey) metabolic features by representing the log2 fold change in altered features and the −log10 adjusted *p*-values with cut off values selected at >1.5 and <0.05, respectively. Upward arrows represent enrichment of features, while downward arrows represent depleted features.

Pooled QC data confirm the stability of the data acquisition system across all the measurements performed in positive and negative ionization acquisition modes (Figure S3b). Distinct clustering patterns were observed, with better separation for the IC_{50} olaparib treatment dose across all cell lines (Figures 4a and S4). Volcano plots indicate the differential number of metabolic features that are significantly altered following exposure to olaparib, relative to control (Figures 4b and S5, Table S5). From a metabolic perspective, we observed that HCC1937 (BRCA1-mutated) cells were the most susceptible to exposure at the IC_{50} olaparib treatment dose, while the MCF7 cells showed a higher number of sig-

nificantly altered metabolic features at the IC_{25} olaparib treatment concentration. Together, these findings show a differential dose- and cell-line-dependent metabolic response to olaparib exposure.

4.4. Amino Acid and Lipid Metabolism Are Significantly Altered in Response to Olaparib Exposure

To analyze specific biomolecular pathways altered by olaparib exposure, we used MetaboAnalyst to identify key metabolic pathways significantly perturbed by olaparib treatment and performed enrichment analysis for both control and treated samples (Figures 5 and S6). Among the pathways ranked in the top ten, we selected altered pathways with a corresponding pathway impact > 0.1, and a *p*-value < 0.05.

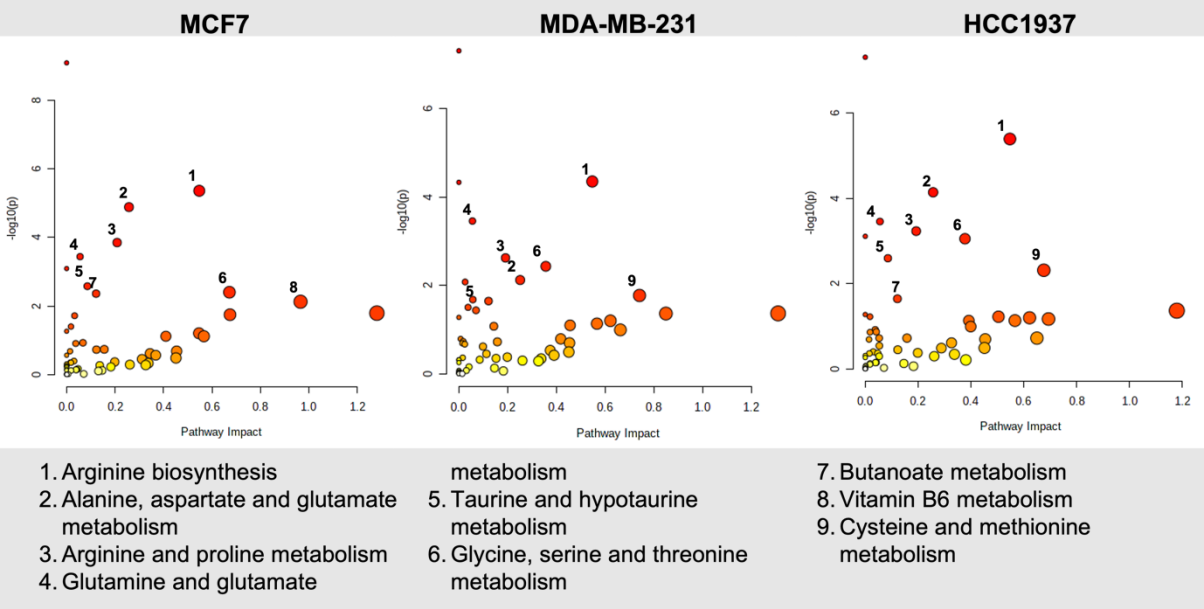

Figure 5. Pathway enrichment analysis of MCF7 (10 μM), MDA-MB-231 (14 μM), and HCC1937 (150 μM) cells following a seven-day exposure to olaparib. Enrichment analysis was based on the hypergeometric test. Topological analysis was based on betweenness centrality. The tight integration method was used by combining genes and metabolites into a single query. A $p < 0.05$, and pathway impact > 0.1 were deemed significant.

Across all cell lines examined, the top ten putative pathways significantly altered in Metaboanalyst (Figure 5, Table S6) were based on amino acid (arginine biosynthesis, glutamine, glycine, serine, and threonine metabolism) and lipid metabolism (butanoate metabolism). Following the identification of metabolic pathways altered by olaparib exposure, we constructed a Venn diagram (Figure S7) to outline common overlapping and cell line-specific altered metabolic features.

Overlapping pathways are mostly represented by amino acid metabolism (glutamine, glutamate, aspartate, alanine, arginine, and proline), suggesting a strong reliance of breast cancer cell metabolism on amino acids under baseline conditions (control samples). Upon olaparib exposure, the same pathways (amino acid metabolism) were among the most significantly altered across all cell lines, while fatty acid (butanoate metabolism) and vitamin B6 metabolism were only significantly perturbed in MCF-7 cells.

Next, we explored individual metabolites that were associated with significantly altered metabolic pathways in response to olaparib exposure and evaluated relative changes in their levels between control and treatment samples. These results are presented through a heatmap clustering analysis (Figure 6). A correlation analysis between each metabolite is shown in Figure S8, and a wider list of compounds specific for each cell type is provided (Table S7).

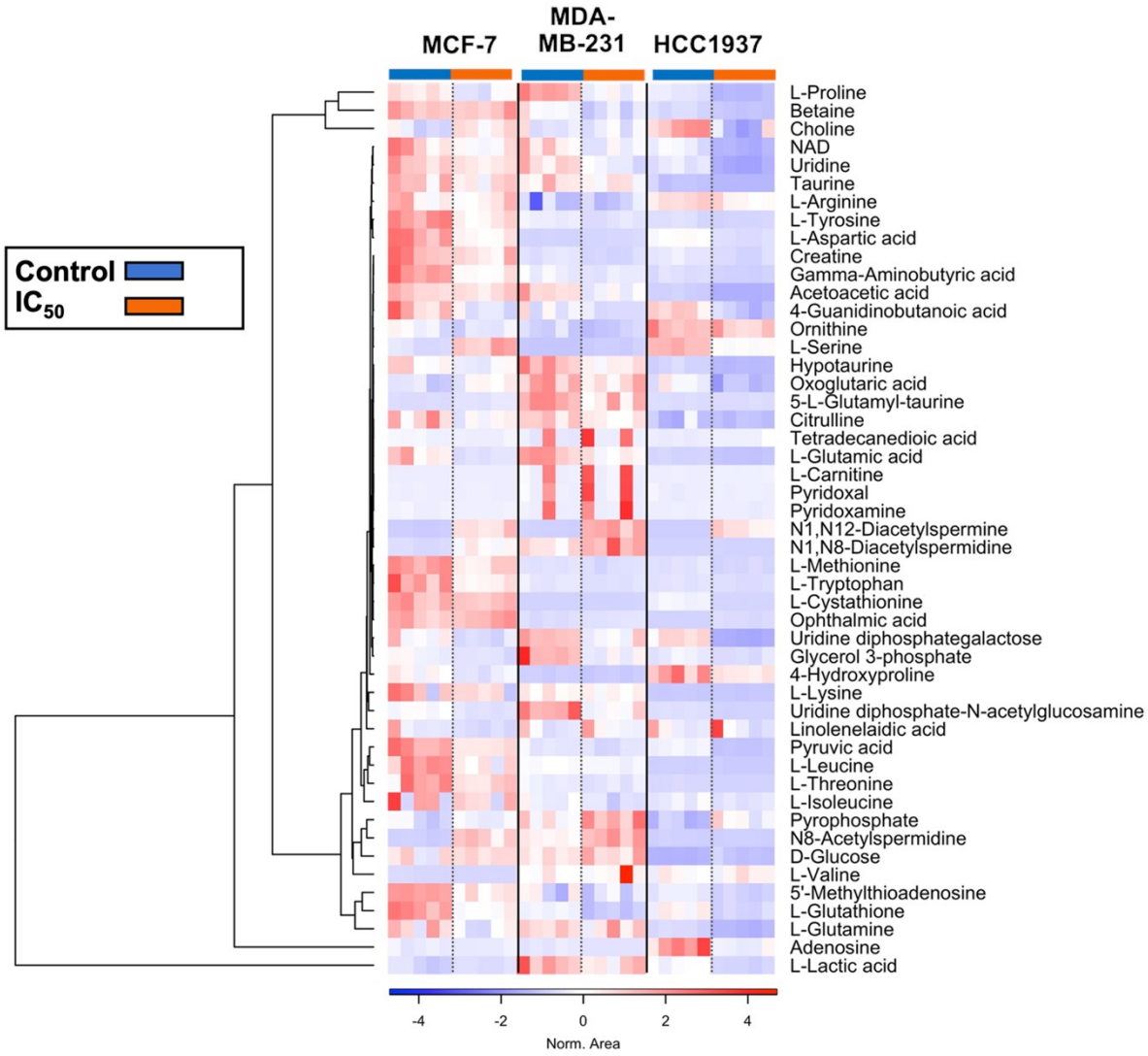

Figure 6. Heatmap cluster analysis of relevant metabolites associated with the pathways altered upon exposure to olaparib in MCF7 (10 μM), MDA-MB-231 (14 μM), and HCC1937 (150 μM) cells for seven days. Clustering and distance function are Ward and Euclidean, respectively. Normalized areas indicate chromatographic peaks areas that have been normalized based on the QC samples to compensate for batch effects.

Multiple amino acids (glutamine, glutamate, arginine, proline, methionine, glycine, threonine, taurine, and hypotaurine) were found to be depleted following olaparib exposure (relative to control) in all cell lines examined. Arginine and proline metabolism were significantly depleted by olaparib exposure, with depletion of their derived polyamines detected in all cell lines examined. Conversely, catabolic products of arginine and proline metabolism (N8-Acetylspermidine, N1-N8-Diacetylspermidine, and N1-N12-Diacetylspermine) were enriched. Elevated levels of serine were observed in MCF7 and MDA-MB-231 cells, while depletion of serine levels was seen in HCC1937 cells.

Alpha-ketoglutarate (α-KG-glutamine-derived intermediate of the TCA cycle) was enriched in MCF7 and depleted in MDA-MB-231 and HCC1937 cells. A negative correlation was observed between α-KG and glutamine levels, and a positive correlation between α-KG, and citric and fumaric acid (TCA cycle intermediates). Aspartate (a TCA cycle product) accumulated in the KRAS-mutant MDA-MB-231 cells, while aspartate depletion was observed in MCF7 and HCC1937 cells. Glucose levels were significantly elevated relative to control samples in HCC1937 cells. Asparagine (a byproduct of aspartate) was absent in MDA-MB-231 cells, while its enrichment was detected in MCF7 and HCC1937 cells. In

parallel, accumulation of AMP was observed in both MCF7 and HCC1937 cell lines, while it was absent in MDA-MB-231 cells, and enrichment of PPi was detected in all cell lines examined following olaparib exposure.

In the case of lipid metabolism, we observed a global depletion of phosphocholines (PC) and phosphoethanolamines (PE) in all cell lines following olaparib treatment. Acylcarnitine levels varied across the cell lines, with an overall enrichment of long (C14–C21) and very-long chain acylcarnitines (>C22) in all cell lines treated with olaparib. Moreover, we observed enriched alpha-linoleic acid (a polyunsaturated fatty acid-PUFA) levels in MCF7 and MDA-MB-231 cells, which was absent in HCC1937 cells.

Compared to non-treated cells, elevated levels of glucose were detected in all cell lines studied following olaparib treatment, while downregulation of most nucleobases was observed. Finally, NAD+ downregulation was detected in all cell lines treated with olaparib.

An overview of the metabolic features altered in response to olaparib exposure is given in Figure 7, where we mapped cell line differences in metabolite levels through the Kyoto Encyclopaedia of Genes and Genomes (KEGG) database. Moreover, in the figure we represented the fitness effect score of metabolic enzymes relative to each Olaparib-treated cell, which have been obtained through a cross-comparison with the Dependency Map Portal (DepMap; Table S8). The fitness effect score measures the effect of knocking out a gene on cell proliferation. A negative score indicates that the knocked-out gene causes a slower cell proliferation, while a positive score is indicative of a consequent enhanced proliferation [21].

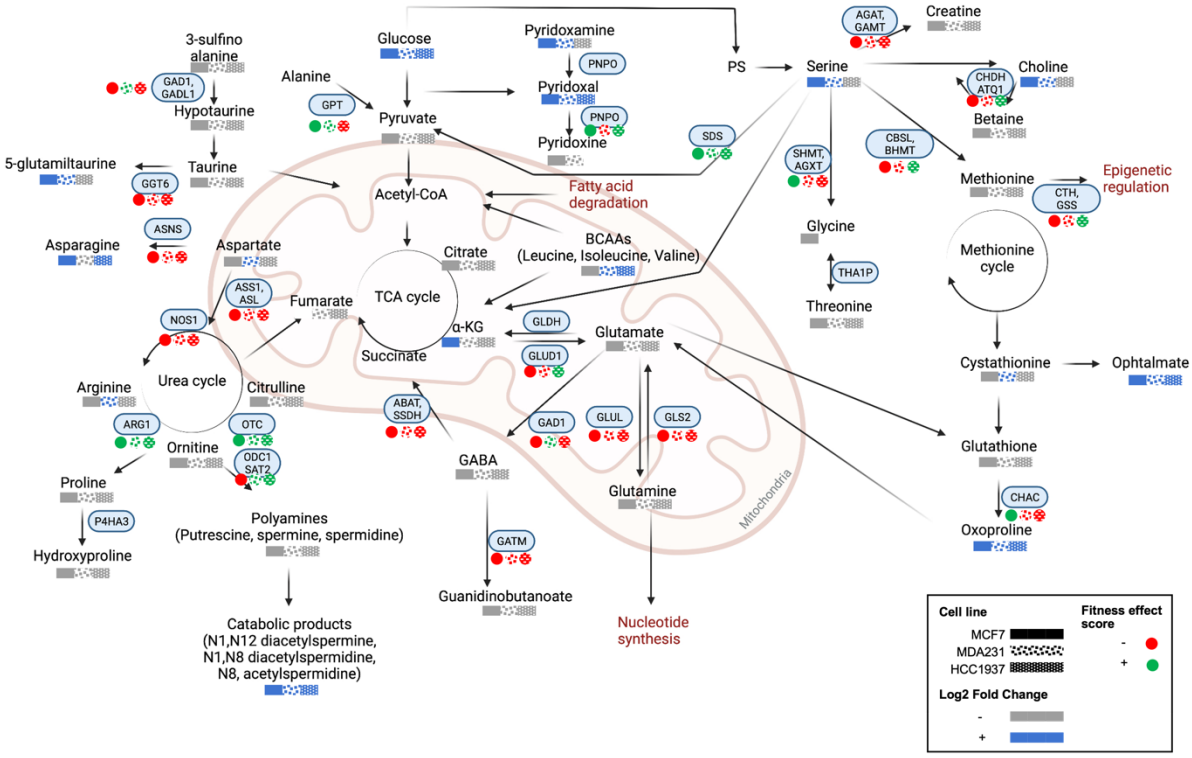

Figure 7. A summary of putatively identified metabolic pathways altered in response to olaparib exposure at IC_{50} doses. Significantly altered features with a Log2 fold change of >1.5 (blue-enriched and grey-depleted). Fitness effect score of metabolic enzymes (light-blue boxes) in relation to PARP expression in each cell line. Positive and negative scores are in green and red, respectively. MCF-7 ( ), MDA-MB-231 ( ), and HCC1937 ( ). Fitness effect score is based on the Chronos algorithm.

5. Discussion

PARP inhibitors have shown promising results in the treatment of metastatic breast cancers harboring germline BRCA1/2 mutations [22,23]. Recent clinical studies have shown evidence of PARP inhibitor efficacy in the management of breast cancer, irrespective of tumor BRCAness. Prior work has shown that BRCA1-mutated cells carrying a TP53 mutation are resistant to treatment with PARP inhibitors [24]. Therefore, additional factors beyond BRCAness may govern sensitivity to PARP inhibition.

In this study we analyzed the sensitivity of two triple-negative (MDA-MB-231 and HCC1937) and MCF-7 (ER+, PR−, HER2−) cell lines to olaparib PARP inhibition (PARP1/2). The rationale for selecting these cell lines was to explore how their different genetic profiles (see Supplementary Table S1) define the observed differential biomolecular perturbations in response to olaparib treatment. Initially, we examined the responsiveness of MCF-7, MDA-MB-231, and HCC1937 cell lines to olaparib exposure using the MTS cell viability assay (Figure 1). Our results show differential sensitivity to olaparib exposure across the cell lines examined, with MCF-7 and MDA-MB-231 showing sensitivity to olaparib treatment at lower micromolar concentrations, and the BRCA1-mutant HCC1937 cell line showing less sensitivity (IC_{50}—150 μM). These findings are in agreement with previous reports of HCC1937 resistance to PARP inhibition, where the identification of predictive biomarkers of response to PARP inhibitor treatments was recommended beyond BRCA1/2 status [24].

Our analysis of γH2AX and p53BP1 DNA DSB immunolabelled foci (Figure 3) showed a higher occurrence of DNA damage foci in HCC1937 cells in comparison with MCF-7 and MDA-MB-231 cells with wild-type BRCA status. These observations suggest that BRCA status does not necessarily translate to olaparib sensitivity, and additional DDR components may define responsiveness. At present, routine clinical decision making surrounding the selection of treatment interventions are based on BRCA status, anatomical location, hormone receptor status and tumor stage, with very limited attention given to other mediators of DDR—namely homologous recombination—known to confer a BRCAness phenotype similar to BRCA 1 or 2 loss. Several recent studies have used whole-genome sequencing or the integration of homologous recombination panel scoring systems to provide an additional framework for predicting responders to PARP inhibitor treatment [25,26].

Genetic biomarkers are routinely used in the clinical stratification of breast cancers and predicting treatment-emergent resistance [27]. While genome-wide studies have improved patient stratification efforts, they lack the potential to account for functional phenotypic effects resulting from protein expression levels, or gain- or loss of function effects. Metabolomics has emerged in the past decade as an additional research toolbox for studying potential biomarkers of breast cancer, with a range of applications ranging from early detection to the discovery of new metabolites and prognostic classification of patients with breast cancer [28].

Our goal in the present study was to apply combined analysis of DNA damage foci formation with global untargeted mass-spectrometry based metabolomics to map the metabolic changes occurring following exposure to olaparib. We examined the baseline differences in cellular metabolism across the cell line panel and extended this evaluation to examine cell-line-dependent response to olaparib treatment. Under baseline cell culture conditions, we found overlapping metabolic features (alanine, aspartate, glutamine, arginine, proline, glycine, serine, and threonine) occurring across all three breast cancer cell lines studies, and metabolic signatures that were unique to specific cell lines (MCF7: sphingolipid and glycerophospholipid metabolism; MDA-MB-231: taurine and hypotaurine metabolism; HCC1937: glyoxylate and dicarboxylate metabolism) (Figures 5 and 6).

Our analysis of metabolites significantly altered in response to olaparib treatment correlate with reports from Bhute et al., where metabolic markers of PARP inhibition were reported as changes in amino acid metabolism (glutamine and alanine), downregulation of osmolyte levels (taurine, and GPC), phosphocreatine, lactate, and pyruvate in MCF7

cells [29]. We reported downregulation of those metabolites in the MDA-MB-231 and HCC1937 cells, while low levels of fumarate were observed only in the HCC1937 cells (Figure 6). Bhute et al. also reported increased NAD+ levels for cells treated with veliparib. In our results, NAD+ levels increased in the MCF7 cells treated with olaparib at the IC_{10} treatment concentration, accompanied by a decrease in NAD+ levels at ascending concentrations of olaparib. Reduced levels of NAD+ were also detected in the MDA-MB-231 and HCC1937 cells at all treatment concentrations. Recent studies have shown that in TNBC cells, olaparib enhances the signaling pathways of other NAD+-dependent deacetylase (i.e., sirtuins) [29,30]. These findings are in agreement with our observation of depleted acetyl-amino acid levels and enrichment of methyl-pyridines, -pyrrolidines, and -nucleosides. Further studies are needed to confirm the divergence of NAD+ flow towards alternative pathways and its association with specific breast cancer subphenotypes.

Glutamine, a precursor for protein, nucleotide, and lipid biosynthesis, is a fundamental amino acid in breast cancer cell metabolism, playing a pivotal role in providing anaplerotic intermediates for the tricarboxylic acid (TCA) cycle [31]. Previous reports have indicated a reduction of glutamine levels only for the TNBC cells after treatment with veliparib, and in the MCF7 cells only in combination with other DDR inhibitors [16]. Our results show reduced glutamine levels in all cell lines treated with olaparib, suggesting increased glutamine utilization. Once internalized by cells, glutamine can be converted to glutamate and alpha-ketoglutarate (α-KG). α-KG—a by-product of isocitrate—is oxidized in the TCA cycle through a reaction catalyzed by isocitrate dehydrogenase (IDH), which is frequently mutated in cancer. Several studies have studied α-KG as an oncometabolite, where elevated levels induce the reversal of enhanced glycolysis through downregulation of the Hypoxia-inducible factor (HIF1), which, following PARP inhibition, leads to cell death [32,33]. Recent findings have shown that mutant IDH—and the consequent synthesis of aberrant α-KG forms—confers a BRCAness phenotype [34], downregulating the expression of the DNA repair enzyme Ataxia-telangiectasia mutated (ATM) kinase [35], altering the methylation status of loci surrounding DNA breaks [36]. Together, these alterations lead to homology-dependent repair (HDR) impairment and increase susceptibility to PARP inhibition. On this basis, the reduced α-KG levels observed in olaparib-treated MDA-MB-231 and HCC1937 cells shows the basis for potential resistance to the anti-proliferative effects of olaparib. The increased utilization of α-KG by HCC1937 cells is paralleled by an increased consumption of serine at ascending doses of olaparib. These observations are consistent with reports that in BRCA1-mutated TNBC cell lines, approximately 50% of α-KG results from the flux of serine metabolism [37].

Glutamine is also a source of nitrogen groups for the synthesis of nucleobases and nucleotides, either directly or through a process involving the transamination of glutamate and the TCA cycle-derived oxaloacetate that generates aspartate [38–40]. Our results show that low levels of glutamine are associated with overall reduction in nucleobase and nucleotide levels. MCF7 and HCC1937 cells showed accumulation of adenosine monophosphate (AMP), which represents a depleted energy and nutrient status of the cells known to activate the metabolic sensor AMP-activated protein kinase (AMPK) leading to cell growth inhibition [41]. Different studies have considered activation of AMPK a metabolic cancer suppressor and an attractive therapeutic target for TNBC [42], however, its signaling network in response to PARP inhibition in different breast cancer cells needs to be established. In opposition to what was observed by Bhute et al., aspartate, a byproduct of the TCA cycle, accumulated in the MDA-MB-231 cells after PARP inhibition compared to its reduction in the MCF7 and HC1937 cells. Lowered plasma aspartate levels have been diagnosed in breast cancer patients, suggesting an increased tumor utilization of this metabolite [43]. Moreover, we observed that aspartate metabolism is relevant both in the baseline model and in response to olaparib, which suggests a role of this metabolite in regulating the different metabolic phenotypes of breast cancer cells. However, its role has been poorly investigated, and little is known about its association with PARP inhibition.

Among the pathways of aspartate utilization, asparagine is converted through the enzyme asparagine synthetase (ASNS). The reaction requires glutamine as a substrate and consumption of adenosine triphosphate (ATP) to produce adenosine monophosphate (AMP) and pyrophosphate (PPi). Physiological levels of asparagine occur at levels of < 0.05 mM in human plasma [44]. Cancer cells harboring mutant KRAS (e.g., MDA-MB-231) possess lower ASNS expression levels, leading to lower baseline aspartate levels explaining the rationale for the lack of aspartate detection in MDA-MB-231 lines [45]. In breast cancer cells, the increased bioavailability of asparagine promotes metastatic progression [46] due to its role in protein synthesis and regulation of amino acid homeostasis [47]. We found elevated asparagine levels in olaparib-treated MCF7 and HCC1937 cells, suggesting a role for asparagine in the observed responses to exposure to PARP inhibitor.

Beyond asparagine synthesis, aspartate amidation through ASNS presents a source of amino building blocks for the synthesis of arginine in the urea cycle, which is in turn responsible for the synthesis of polyamines catalyzed by ornithine decarboxylase (ODC). Polyamine accumulation has previously been correlated with the increased proliferation of both hormone-dependent and independent breast cancer cells [48], and was recently found to contribute to BRCA1-mediated DNA repair [49]. Moreover, metabolic profiling of plasma samples from patients with TNBC revealed an increase of diacetyl spermines associated with elevated expression of MYC, a well-known oncogene driving TNBC development and proliferation. Here, we found elevated diacetyl spermine levels following olaparib treatment in both TNBC and non-TNBC cells, suggesting an upregulation of polyamine catabolism, irrespective of cell line BRCA- and hormone receptor status. Parallel to their relevance in cellular metabolism, amino acids also serve as biological buffers through regulation of cellular pH. Low extracellular pH is associated with positively charged amino acids and a known hallmark of cancer arising from enhanced glycolysis, production and altered lactate metabolism, resulting in altered mTOR pathway activation, ultimately regulating cancer cell metabolism [50,51].

Glutathione (GSH) is involved in the protection against ROS and regulation of intracellular redox homeostasis. Elevated GSH levels have previously been reported in TNBC compared to luminal breast cancers, suggesting the relevance of GSH to our observations of lower sensitivity to olaparib in TNBC cell lines [17,52].

Lipids mediate various cellular biological functions, including energy storage, cell membrane structural composition and signal transduction, the increased biosynthesis of which is a marker of metabolic rewiring observed in malignant breast cancers [53,54]. Our findings show downregulation of fatty acid biosynthesis following olaparib treatment, with a reduction in phospholipid levels, including lysophosphatidylcholines and glycerolphosphocholines, in all cell lines. Poly-unsaturated fatty acids (PUFAs) have previously been implicated in MCF7 and MDA-MB-231 cell apoptosis through the induction of lipid peroxidation and altered cellular redox state [55]. Moreover, elevated PUFA levels have been associated with the proteolytic cleavage of PARP and its inhibition, leading to cell death [56]. On this basis, the reduced PUFA levels observed in HCC1937 cells may indicate their resistance to olaparib treatment. Only a limited number of studies have reported a correlation between PUFAs and breast cancer subphenotypes, requiring further validation by additional studies.

Future targeted metabolomics studies using additional TNBC cell lines and clinical tumor clinical specimens are required to validate our observations. Validation of our findings could define prognostic biomarkers that will aid evaluation of patient prognosis in the clinical setting and enable the implementation of precision medicine in the management of breast cancer.

6. Conclusions

Our data show differential sensitivity of breast cancer cell lines to olaparib treatment that was dose-dependent and demonstrated the increased sensitivity of TNBC cells to DNA damage foci accumulation. The application of metabolomics to the study of breast

cancer remains in its infancy, with only a handful of studies reporting combined metabolomics and phenotypic analyses. Data acquired from metabolomics analysis can be validated against routine molecular biology and phenotypic assays, providing a powerful platform for biomarker detection or the discovery of novel actionable pathways for drug development.

Our results show that fingerprinting the metabolic profile of cells can be a powerful tool for uncovering potential oncometabolites or mechanisms giving rise to chemoresistance. Findings from such studies may provide potential additional actionable targets for modulating response to drug treatment or the design of new drug combinations that will overall enhance DNA damage efficacy, ultimately improving patient response to radiotherapy and adjuvant chemotherapy.

Supplementary Materials: The following supporting information can be downloaded at: https://www.mdpi.com/article/10.3390/cancers14153661/s1, Figure S1: The formation of p53BP1 foci in response to treatment with either growth medium or medium containing Olaparib at various doses, Figure S2: The formation of γH2AX foci formation in response to treatment with either growth medium or medium containing olaparib at various doses, Figure S3: Untargeted mass spectrometry-based metabolomics and data analysis pipeline (a- created in Biorender.com). Global metabolic features identified in MCF7, MDA-MB-231 and HCC1937 upon exposure to IC10, IC25 and IC50 olaparib doses for seven days acquired in positive and negative ionization mode (b), Figure S4: PCA pairwise analysis of untargeted metabolomics data collected, in both positive and negative mode, from MCF7, MDA-MB-231, and HCC1937 cells treated with IC10, IC25 and IC50 olaparib treatment doses in positive and negative ionization modes, Figure S5: Volcano plots showing the log2 fold change and the -log10 adjusted p-values in metabolite levels induced by treatment with different doses of Olaparib (IC10, IC25, and IC50) in MCF7, MDA-MB-231 and HCC1937 cells, Figure S6: Enrichment analysis of non-treated MCF7, MDA-MB-231 and HCC1937 cells, Figure S7: Venn diagram representing the metabolic pathways in MCF7, MDA-MB-231 and HCC1937 cells, Figure S8: Pearson's correlation analysis between the relevant metabolites identified within each different breast cancer cell line, Table S1: Cell lines used in this study and their corresponding clinicopathologic profiles, Table S2: Corresponding elution gradient used for the chromatographic separation of metabolite extracts, Table S3: Normality test for cell viability and immunofluorescence quantification data, Table S4: ANOVA analysis of olaparib dose-dependent DNA DSB immunofoci formation, Table S5: Global differential number of altered metabolites for samples treated with IC10, IC25 and IC50 of Olaparib and their relative control (non-treated) samples, Table S6: Metabolic pathways in different breast cancer cells (MCF7, MDA-MB-231, and HCC1937) before and after treatment with IC50 dose of Olaparib, Table S7: Classification of the metabolites identified in MCF7, MDA-MB-231 and HCC1937 at all olaparib doses (IC10, IC25 and IC50) after seven days treatment, Table S8: Effect scores of enriched metabolic genes in MCF-7, MDA-MB-231 and HCC1937 cells evaluated through the Dependency Map Portal (DepMap) database. Fitness effect score is based on the Chronos algorithm.

Author Contributions: Conceptualization: Z.R., N.J.W.R. and D.B.; Investigation: D.B., Y.H., G.F., N.J.W.R. and Z.R.; Methodology: D.B., Y.H., L.v.d.D., G.F., Z.R. and N.J.W.R.; Analysis: D.B., Y.H., N.J.W.R., Z.R. and L.v.d.D.; Writing original draft: Z.R. and D.B.; Visualization: D.B., L.v.d.D., N.J.W.R. and Z.R.; Writing—reviewing and editing: D.B., Y.H., L.v.d.D., G.F., N.J.W.R. and Z.R.; Funding acquisition: N.J.W.R. and Z.R. All authors have read and agreed to the published version of the manuscript.

Funding: This work was supported by Tenovus Scotland (Z.R.), the Royal Society of Edinburgh Research Reboot (Z.R.), and the UK Engineering and Physical Sciences Research Council (Z.R., EPSRC EP/V028960/1). For the purpose of open access, the authors have applied for a CC BY copyright license to any Author Accepted Manuscript version arising from this submission.

Institutional Review Board Statement: Not applicable.

Informed Consent Statement: Not applicable.

Data Availability Statement: The datasets generated and used/or analyzed are available from the corresponding authors upon request.

Acknowledgments: The authors acknowledge the Strathclyde Centre for Molecular Biology (SCMB) for providing access to mass spectrometry facilities.

Conflicts of Interest: The authors declare no conflict of interest.

References

1. Gueble, S.E.; Bindra, R.S. Oncometabolites as Regulators of DNA Damage Response and Repair. *Semin. Radiat. Oncol.* **2021**, *32*, 82–94. https://doi.org/10.1016/j.semradonc.2021.09.004.
2. Huang, R.; Zhou, P.-K. DNA damage repair: Historical perspectives, mechanistic pathways and clinical translation for targeted cancer therapy. *Signal Transduct. Target. Ther.* **2021**, *6*, 254. https://doi.org/10.1038/s41392-021-00648-7.
3. He, C.; Kawaguchi, K.; Toi, M. DNA damage repair functions and targeted treatment in breast cancer. *Breast Cancer* **2020**, *27*, 355–362. https://doi.org/10.1007/s12282-019-01038-2.
4. Ottini, L.; Rizzolo, P.; Silvestri, V.; Falchetti, M. Inherited and acquired alterations in development of breast cancer. *Appl. Clin. Genet.* **2011**, *4*, 145–158. https://doi.org/10.2147/TACG.S13226.
5. Godet, I.; Gilkes, D.M. BRCA1 and BRCA2 mutations and treatment strategies for breast cancer. *Integr. Cancer Sci. Ther.* **2017**, *4*. https://doi.org/10.15761/icst.1000228.
6. O'Neil, N.; Bailey, M.L.; Hieter, P. Synthetic lethality and cancer. *Nat. Rev. Genet.* **2017**, *18*, 613–23.
7. Li, S.; Topatana, W.; Juengpanich, S.; Cao, J.; Hu, J.; Zhang, B.; Ma, D.; Cai, X.; Chen, M. Development of synthetic lethality in cancer: Molecular and cellular classification. *Signal Transduct. Target. Ther.* **2020**, *5*, 241. https://doi.org/10.1038/s41392-020-00358-6.
8. Lord, C.J.; Tutt, A.N.; Ashworth, A. Synthetic Lethality and Cancer Therapy: Lessons Learned from the Development of PARP Inhibitors. *Annu. Rev. Med.* **2015**, *66*, 455–470. https://doi.org/10.1146/annurev-med-050913-022545.
9. Cortesi, L.; Rugo, H.S.; Jackisch, C. An Overview of PARP Inhibitors for the Treatment of Breast Cancer. *Target. Oncol.* **2021**, *16*, 255–282. https://doi.org/10.1007/s11523-021-00796-4.
10. FDA. FDA Approves Olaparib for Adjuvant Treatment of High-Risk Early Breast Cancer 2022. Available online: https://www.fda.gov/drugs/resources-information-approved-drugs/fda-approves-olaparib-adjuvant-treatment-high-risk-early-breast-cancer, accessed on May 20th 2022
11. Pavlova, N.N.; Thompson, C.B. The Emerging Hallmarks of Cancer Metabolism. *Cell Metab.* **2016**, *23*, 27–47. https://doi.org/10.1016/j.cmet.2015.12.006.
12. Maria, R.M.; Altei, W.F.; Selistre-De-Araujo, H.S.; Colnago, L.A. Impact of chemotherapy on metabolic reprogramming: Characterization of the metabolic profile of breast cancer MDA-MB-231 cells using 1 H HR-MAS NMR spectroscopy. *J. Pharm. Biomed. Anal.* **2017**, *146*, 324–328. https://doi.org/10.1016/j.jpba.2017.08.038.
13. Gandhi, N.; Das, G. Metabolic Reprogramming in Breast Cancer and Its Therapeutic Implications. *Cells* **2019**, *8*, 89. https://doi.org/10.3390/cells8020089.
14. Palaskas, N.; Larson, S.M.; Schultz, N.; Komisopoulou, E.; Wong, J.; Rohle, D.; Campos, C.; Yannuzzi, N.; Osborne, J.R.; Linkov, I.; et al. 18F-fluorodeoxy-glucose positron emission tomography marks MYC-overexpressing human basal-like breast cancers. *Cancer Res.* **2011**, *71*, 5164–5174.
15. Turgeon, M.; Perry, N.J.S.; Poulogiannis, G. DNA Damage, Repair, and Cancer Metabolism. *Front. Oncol.* **2018**, *8*, 15.
16. Bhute, V.J.; Ma, Y.; Bao, X.; Palecek, S.P. The Poly (ADP-Ribose) Polymerase Inhibitor Veliparib and Radiation Cause Significant Cell Line Dependent Metabolic Changes in Breast Cancer Cells. *Sci. Rep.* **2016**, *6*, 36061. https://doi.org/10.1038/srep36061.
17. Tang, X.; Lin, C.-C.; Spasojevic, I.; Iversen, E.S.; Chi, J.-T.; Marks, J.R. A joint analysis of metabolomics and genetics of breast cancer. *Breast Cancer Res.* **2014**, *16*, 415. https://doi.org/10.1186/s13058-014-0415-9.
18. Huang, A.; Garraway, L.A.; Ashworth, A.; Weber, B. Synthetic lethality as an engine for cancer drug target discovery. *Nat. Rev. Drug Discov.* **2019**, *19*, 23–38.
19. Mah, L.; Karagiannis, T.C. Gammah2ax: A sensitive molecular marker of DNA damage and repair. *Leukemia* **2010**, *24*, 679–686.
20. Schultz, L.B.; Chehab, N.H.; Malikzay, A.; Halazonetis, T.D. P53 Binding Protein 1 (53bp1) Is an Early Participant in the Cellular Response to DNA Double-Strand Breaks. *J. Cell Biol.* **2000**, *151*, 1381–1390. https://doi.org/10.1083/jcb.151.7.1381.
21. Dempster, J.M.; Boyle, I.; Vazquez, F.; Root, D.E.; Boehm, J.S.; Hahn, W.C.; Tsherniak, A.; McFarland, J.M. Chronos: A cell population dynamics model of CRISPR experiments that improves inference of gene fitness effects. *Genome Biol.* **2021**, *22*, 343. https://doi.org/10.1186/s13059-021-02540-7.
22. Robson, M.; Im, S.A.; Senkus, E.; Xu, B.; Domchek, S.M.; Masuda, N.; Delaloge, S.; Li, W.; Tung, N.; Armstrong, A.; et al. Olaparib for Metastatic Breast Cancer in Patients with a Germline BRCA Mutation. *N. Engl. J. Med.* **2017**, *377*, 523–533. https://doi.org/10.1056/nejmoa1706450.
23. AstraZeneca. Lynparza Approved in the US as Adjuvant Treatment for Patients with Germline BRCA-Mutated HER2-Negative High-Risk Early Breast Cancer 2022. Available online: https://www.astrazeneca.com/media-centre/press-releases/2022/lynparza-approved-in-the-us-as-adjuvant-treatment-for-patients-with-germline-brca-mutated-her2-negative-high-risk-early-breast-cancer.html, accessed on May 25th 2022.
24. Keung, M.Y.; Wu, Y.; Badar, F.; Vadgama, J.V. Response of Breast Cancer Cells to PARP Inhibitors Is Independent of BRCA Status. *J. Clin. Med.* **2020**, *9*, 940. https://doi.org/10.3390/jcm9040940.
25. Davies, H.; Glodzik, D.; Morganella, S.; Yates, L.R.; Staaf, J.; Zou, X.; Ramakrishna, M.; Martin, S.; Boyault, S.; Sieuwerts, A.M.; et al. HRDetect is a predictor of BRCA1 and BRCA2 deficiency based on mutational signatures. *Nat. Med.* **2017**, *23*, 517–525. https://doi.org/10.1038/nm.4292.

26. McGrail, D.J.; Lin, C.C.-J.; Garnett, J.; Liu, Q.; Mo, W.; Dai, H.; Lu, Y.; Yu, Q.; Ju, Z.; Yin, J.; et al. Improved prediction of PARP inhibitor response and identification of synergizing agents through use of a novel gene expression signature generation algorithm. *NPJ Syst. Biol. Appl.* **2017**, *3*, 8. https://doi.org/10.1038/s41540-017-0011-6.
27. Harbeck, N.; Penault-Lorca, F.; Cortes, J.; Gnant, M.; Houssami, N.; Poortmans, P.; Ruddy, K.; Tsang, J.; Cardoso, F. Breast cancer. *Nature* **2019**, *5*, 6.
28. Hart, C.D.; Tenori, L.; Luchinat, C.; Di Leo, A. Metabolomics in Breast Cancer: Current Status and Perspectives. *Nov. Biomark. Contin. Breast Cancer* **2016**, *882*, 217–234. https://doi.org/10.1007/978-3-319-22909-6_9.
29. Bhute, V.J.; Palecek, S.P. Metabolic responses induced by DNA damage and poly (ADP-ribose) polymerase (PARP) inhibition in MCF-7 cells. *Metabolomics* **2015**, *11*, 1779–1791. https://doi.org/10.1007/s11306-015-0831-6.
30. Gajan, A.; Sarma, A.; Kim, S.; Gurdziel, K.; Wu, G.S.; Shekhar, M.P. Analysis of Adaptive Olaparib Resistance Effects on Cisplatin Sensitivity in Triple Negative Breast Cancer Cells. *Front. Oncol.* **2021**, *11*, 2857. https://doi.org/10.3389/fonc.2021.694793.
31. Najumudeen, A.K.; CRUK Rosetta Grand Challenge Consortium; Ceteci, F.; Fey, S.K.; Hamm, G.; Steven, R.T.; Hall, H.; Nikula, C.J.; Dexter, A.; Murta, T.; et al. The amino acid transporter SLC7A5 is required for efficient growth of KRAS-mutant colorectal cancer. *Nat. Genet.* **2021**, *53*, 16–26. https://doi.org/10.1038/s41588-020-00753-3.
32. A Tennant, D.; Frezza, C.; MacKenzie, E.D.; Nguyen, Q.D.; Zheng, L.; A Selak, M.; Roberts, D.L.; Dive, C.; Watson, D.G.; O Aboagye, E.; et al. Reactivating HIF prolyl hydroxylases under hypoxia results in metabolic catastrophe and cell death. *Oncogene* **2009**, *28*, 4009–4021. https://doi.org/10.1038/onc.2009.250.
33. Scalia, M.; Satriano, C.; Greca, R.; Stella, A.M.G.; Rizzarelli, E.; Spina-Purrello, V. PARP-1 Inhibitors DPQ and PJ-34 Negatively Modulate Proinflammatory Commitment of Human Glioblastoma Cells. *Neurochem. Res.* **2012**, *38*, 50–58. https://doi.org/10.1007/s11064-012-0887-x.
34. Sulkowski, P.L.; Corso, C.D.; Robinson, N.D.; Scanlon, S.E.; Purshouse, K.R.; Bai, H.; Liu, Y.; Sundaram, R.K.; Hegan, D.C.; Fons, N.R.; et al. 2-Hydroxyglutarate produced by neomorphic IDH mutations suppresses homologous recombination and induces PARP inhibitor sensitivity. *Sci. Transl. Med.* **2017**, *9*, eaal2463. https://doi.org/10.1126/scitranslmed.aal2463.
35. Inoue, S.; Li, W.Y.; Tseng, A.; Beerman, I.; Elia, A.J.; Bendall, S.C.; Lemonnier, F.; Kron, K.J.; Cescon, D.W.; Hao, Z.; et al. Mutant IDH1 Downregulates ATM and Alters DNA Repair and Sensitivity to DNA Damage Independent of TET2. *Cancer Cell* **2016**, *30*, 337–348. https://doi.org/10.1016/j.ccell.2016.05.018.
36. Sulkowski, P.L.; Oeck, S.; Dow, J.; Economos, N.G.; Mirfakhraie, L.; Liu, Y.; Noronha, K.; Bao, X.; Li, J.; Shuch, B.M.; et al. Oncometabolites suppress DNA repair by disrupting local chromatin signalling. *Nature* **2020**, *582*, 586–591. https://doi.org/10.1038/s41586-020-2363-0.
37. Possemato, R.; Marks, K.M.; Shaul, Y.D.; Pacold, M.E.; Kim, D.; Birsoy, K.; Sethumadhavan, S.; Woo, H.-K.; Jang, H.G.; Jha, A.K.; et al. Functional genomics reveal that the serine synthesis pathway is essential in breast cancer. *Nature* **2011**, *476*, 346–350. https://doi.org/10.1038/nature10350.
38. DeBerardinis, R.; Cheng, T. Q's next: The diverse functions of glutamine in metabolism, cell biology and cancer. *Oncogene* **2010**, *29*, 313–324.
39. Okazaki, A.; Gameiro, P.A.; Christodoulou, D.; Laviollette, L.; Schneider, M.; Chaves, F.; Stemmer-Rachamimov, A.; Yazinski, S.A.; Lee, R.; Stephanopoulos, G.; et al. Glutaminase and poly(ADP-ribose) polymerase inhibitors suppress pyrimidine synthesis and VHL-deficient renal cancers. *J. Clin. Investig.* **2017**, *127*, 1631–1645. https://doi.org/10.1172/jci87800.
40. Son, J.; Lyssiotis, C.A.; Ying, H.; Wang, X.; Hua, S.; Ligorio, M.; Perera, R.M.; Ferrone, C.R.; Mullarky, E.; Shyh-Chang, N.; et al. Glutamine supports pancreatic cancer growth through a KRAS-regulated metabolic pathway. *Nature* **2013**, *496*, 101–105. https://doi.org/10.1038/nature12040; Erratum in *Nature* **2013**, *499*, 504.
41. Høyer-Hansen, M.; Jäättelä, M. AMP-Activated Protein Kinase: A Universal Regulator of Autophagy? *Autophagy* **2007**, *3*, 381–383. https://doi.org/10.4161/auto.4240.
42. Cao, W.; Li, J.; Hao, Q.; Vadgama, J.V.; Wu, Y. AMP-activated protein kinase: A potential therapeutic target for triple-negative breast cancer. *Breast Cancer Res.* **2019**, *21*, 29. https://doi.org/10.1186/s13058-019-1107-2.
43. Xie, G.; Zhou, B.; Zhao, A.; Qiu, Y.; Zhao, X.; Garmire, L.; Shvetsov, Y.B.; Yu, H.; Yen, Y.; Jia, W. Lowered circulating aspartate is a metabolic feature of human breast cancer. *Oncotarget* **2015**, *6*, 33369–33381. https://doi.org/10.18632/oncotarget.5409.
44. Stegink, L.; Filer, L.J., Jr.; Brummel, M.C.; Baker, G.L.; Krause, W.L.; Bell, E.F.; Ziegler, E.E. Plasma amino acid concentrations and amino acid ratios in normal adults and adults heterozygous for phenylketonuria ingesting a hamburger and milk shake meal. *Am. J. Clin. Nutr.* **1991**, *53*, 670–675.
45. Gwinn, D.M.; Lee, A.G.; Briones-Martin-Del-Campo, M.; Conn, C.S.; Simpson, D.R.; Scott, A.I.; Le, A.; Cowan, T.M.; Ruggero, D.; Sweet-Cordero, E.A. Oncogenic KRAS Regulates Amino Acid Homeostasis and Asparagine Biosynthesis via ATF4 and Alters Sensitivity to L-Asparaginase. *Cancer Cell* **2018**, *33*, 91–107.e6. https://doi.org/10.1016/j.ccell.2017.12.003.
46. Knott, S.R.V.; Wagenblast, E.; Khan, S.; Kim, S.Y.; Soto, M.; Wagner, M.; Turgeon, M.-O.; Fish, L.; Erard, N.; Gable, A.L.; et al. Asparagine bioavailability governs metastasis in a model of breast cancer. *Nature* **2018**, *554*, 378–381. https://doi.org/10.1038/nature25465.
47. Krall, A.S.; Xu, S.; Graeber, T.G.; Braas, D.; Christofk, H.R. Asparagine promotes cancer cell proliferation through use as an amino acid exchange factor. *Nat. Commun.* **2016**, *7*, 11457. https://doi.org/10.1038/ncomms11457.
48. Kim, I.; Manni, A.; Lynch, J.; Demers, L. Polyamine involvement in the secretion and action of TGF-α in hormone sensitive human breast cancer cells in culture. *Breast Cancer Res. Treat.* **1991**, *18*, 83–91. https://doi.org/10.1007/bf01980970.

49. Lee, C.-Y.; Su, G.-C.; Huang, W.-C.; Ko, M.-Y.; Yeh, H.-Y.; Chang, G.-D.; Lin, S.-J.; Chi, P. Promotion of homology-directed DNA repair by polyamines. *Nat. Commun.* **2019**, *10*, 65. https://doi.org/10.1038/s41467-018-08011-1.
50. Zhang, X.; Lin, Y.; Gillies, R.J. Tumor pH and Its Measurement. *J. Nucl. Med.* **2010**, *51*, 1167–1170. https://doi.org/10.2967/jnumed.109.068981.
51. Balgi, A.D.; Diering, G.H.; Donohue, E.; Lam, K.; Fonseca, B.D.; Zimmerman, C.; Numata, M.; Roberge, M. Regulation of mTORC1 Signaling by pH. *PLoS ONE* **2011**, *6*, e21549. https://doi.org/10.1371/journal.pone.0021549.
52. Lien, E.C.; Lyssiotis, C.A.; Juvekar, A.; Hu, H.; Asara, J.M.; Cantley, L.C.; Toker, A. Glutathione biosynthesis is a metabolic vulnerability in PI(3)K/Akt-driven breast cancer. *Nat. Cell Biol.* **2016**, *18*, 572–578. https://doi.org/10.1038/ncb3341.
53. Beckonert, O.; Bonk, U.; Leibfritz, D. Visualizing metabolic changes in breast-cancer tissue using1H-NMR spectroscopy and self-organizing maps. *NMR Biomed.* **2003**, *16*, 1–11. https://doi.org/10.1002/nbm.797.
54. Cao, M.D.; Döpkens, M.; Krishnamachary, B.; Vesuna, F.; Gadiya, M.M.; Loenning, P.E.; Bhujwalla, Z.M.; Gribbestad, I.S.; Glunde, K. Glycerophosphodiester phosphodiesterase domain containing 5 (GDPD5) expression correlates with malignant choline phospholipid metabolite profiles in human breast cancer. *NMR Biomed.* **2012**, *25*, 1033–1042. https://doi.org/10.1002/nbm.2766.
55. Deshpande, R.; Mansara, P.; Suryavanshi, S.; Kaul-Ghanekar, R. Alpha-linolenic acid regulates the growth of breast and cervical cancercell lines through regulation of NO release and induction of lipidperoxidation. *J. Mol. Biochem.* **2013**, *2*, 6–17.
56. Kim, J.-Y.; Park, H.D.; Park, E.; Chon, J.-W.; Park, Y.K. Growth-Inhibitory and Proapoptotic Effects of Alpha-Linolenic Acid on Estrogen-Positive Breast Cancer Cells. *Ann. N. Y. Acad. Sci.* **2009**, *1171*, 190–195. https://doi.org/10.1111/j.1749-6632.2009.04897.x.